32nd EPS Conference on Plasma Phys. Tarragona, 27 June - 1 July 2005 ECA Vol.29C, P-4.042 (2005)

GYRO Simulations of Core Momentum Transport in DIII-D and JET Plasmas

R.V.Budny[1], J.Candy[2], R.E.Waltz[2],
and contributors to the DIII-D and JET-EFDA* work programs
[1]*Princeton Plasma Physics Laboratory, P.O. Box 451, Princeton, NJ 08543, USA,*
[2]*General Atomics, P.P Box 85608 San Diego, CA 92186, USA,*

Abstract

Momentum, energy, and particle transport in DIII-D and JET ELMy H-mode plasmas is simulated with GYRO and compared with measurements analyzed using TRANSP. The simulated transport depends sensitively on the $\nabla(T_i)$ turbulence drive and the $\nabla(E_r)$ turbulence suppression inputs. With their nominal values indicated by measurements, the simulations over-predict the momentum and energy transport in the DIII-D plasmas, and under-predict in the JET plasmas. Reducing $|\nabla(T_i)|$ and increasing $|\nabla(E_r)|$ by up to 15% leads to approximate agreement (within a factor of two) for the DIII-D cases. For the JET cases, increasing $|\nabla(T_i)|$ or reducing $|\nabla(E_r)|$ results in approximate agreement for the energy flow, but the ratio of the simulated energy and momentum flows remains higher than measurements by a factor of 2-4.

Introduction - Turbulent core transport is largely understood to arise from ion temperature gradient (ITG) and trapped electron mode (TEM) long wavelength instabilities. Most previous studies have focused on energy transport to the neglect of particle and momentum transport. We focus here on the latter. It is important to understand the radial transport of plasma momentum since future burning plasmas are expected to have relatively smaller external torques than are typical with present NBI-heated plasmas. Toroidal momentum and its shear play important roles. Besides rotation influencing locked modes, shear appears to play a major role in suppressing turbulence.

The gyrokinetic code GYRO [1] is being used to simulate microturbulence in a variety of plasma regimes. We believe GYRO contains the comprehensive physics needed for physically accurate and realistic simulations of core transport: basic ITG/TEM modes, kinetic treatment of both trapped and passing electrons including electromagnetic effects, $E\times B$ shear, non-zero ρ_s, profile shear, toroidal rotational shear (Kelvin-Helmholtz drive), ion and electron pitch angle collisions, species and momentum conserving Krook ion-ion collisions, real geometry and experimental profile inputs. GYRO also has the capability to study neoclassical transport. Nonlinear simulations are able to predict microturbulent energy, particle, and momentum transport.

Recent improvements to GYRO have added the capability to treat multiple ion species. This capability was used in flux-tube geometry to study physics of particle transport and pinches [2]. Also recently tools for generating the GYRO input profiles for multiple ion species from TRANSP runs were developed, and the ability to simulate microturbulent radial flows of angular momentum were added. This paper uses these features for the first nonlinear gyrokinetic simulations of angular momentum, energy, and particle transport with two-ion species, and compares these with experimental results.

Plasmas Studied - We used these new GYRO features to study a variety of plasma regimes (L-mode, H-mode, and ITB) from the DIII-D, JET, and JT-60U tokamaks. Here we focus on DIII-D and JET ELMy H-mode plasmas. The DIII-D plasmas were from a series of experiments to compare transport in co-I_p and counter-I_p NBI [3]. Plasma shots with well matched profiles, except for differing $\rho_s \equiv c_s/\Omega_i$ (with $c_s \equiv \sqrt{(T_e/m_i)}$ and Ω_i the main-ion gyro frequency) were shown to exhibit Bohm scaling with counter-I_p NBI and gyro-Bohm with co-I_p NBI. We focus on the co and counter pair with lowest and nearly matching $\rho_* \equiv \rho_s/a$. A new analysis of the charge exchange data was done for our study.A summary of plasma parameters is given in Table I. The radial domains chosen for the GYRO simulations were typically 15-40 % of the minor radius, centered around specified values of $\hat{r}$ (the normalized midplane minor radius used as a flux surface label) in the Table. We chose the domains to be sufficiently far from the magnetic axis to have appreciable transport, and far from the top of the pedestal region to avoid the steep

gradients and other complications of pedestal physics. The P_{NBI} was modulated in one of the plasmas (82205) to lower the average heating power for comparisons with other shots. The plasma profiles, except for v_{tor} (with opposite direction relative to I_p) and the radial electric field profile E_r, were similar to those of 99251 with significantly higher P_{NBI}. This indicates a lower energy confinement time τ_E for the counter-I_p plasma.

Two JET ELMy H-mode plasmas were also studied. One had a long-duration DT-NBI phase achieving $Q_{DT} = 0.19$ [4] This plasma is especially interesting as a prototype of base-line plasmas planned for ITER. The other is a D-NBI plasma with trace Ar gas injection and good energy confinement [5]. The JET plasmas have lower ρ_* than the DIII-D ones, even at the larger $\hat{r}$ chosen.

shot	DIII-D 82205	DIII-D 99251	JET 42982	JET 53030
type	co-I_p NBI	ctr-I_p NBI	record Q_{DT}	Ar seeded
R_0, a [m]	1.76, 0.60	1.76, 0.60	2.99, 0.75	2.98, 0.70
I_p [MA], B [T]	1.35, 2.0	1.35, 2.0	3.8, 4.0	2.5, 2.5
P_{NBI} [MW]	4.8-7.2	9.0	21.5	12.4
time [s]	2.5	2.2	16.4	21.5
$\hat{r}$	0.60	0.60	0.75	0.70
$\rho_* \equiv \rho_s(\hat{r})/a$	0.0411	0.0403	0.0164	0.0168
$E_r(\hat{r})$ [kV/m]	+40.8	-40.5	+119.0	+54.6
$\nabla(E_r)$ $[kV/m^2]$	-90.0	+52	-140	-138
$\chi_\phi(\hat{r})^{transp}$ $[m^2/s]$	1.0-1.2	1.2	1.1	0.3
$\chi_i(\hat{r})^{transp}$ $[m^2/s]$	0.7-1.1	1.15	1.7	0.9
$\chi_{eff}(\hat{r})^{transp}$ $[m^2/s]$	1.3-1.7	0.90	3.8	1.6
Γ_E^{transp} [MW]	3.5-4.5	3.4-4.3	16.8	6.0
Γ_ϕ^{transp} [Nt-m]	2.8-4.8	-(3.3-4.1)	19.0	8.0
Γ_{el}^{transp} [MW/keV]	0.1	0.08	0.20	0.11
$k_\theta \rho_s$ (max)	0.506	0.502	0.401	0.496
γ_{lin} $[c_s/a]$	0.190	0.227	0.109	0.164
$\gamma_{E\times B}$ $[c_s/a]$	0.068	-0.098	0.078	0.126
ω_{lin} $[c_s/a]$	-0.432	-0.284	-0.223	-0.311
$\lvert\nabla(T_i)^{used}\rvert/\lvert\nabla(T_i)^{transp}\rvert$	0.85	0.85	1.00	1.00
$\lvert\nabla(E_r)^{used}\rvert/\lvert\nabla(E_r)^{transp}\rvert$	1.00	1.00	0.90	0.25
$\chi_{E;\ ion-1,\ ion-2,\ el}^{gyro}$ $[(c_s/a)\rho_s^2]$	1.7,-0.1, 0.7	0.7, 0.3, 0.2	1.9, 3.6, 0.6	2.6, 2.2, 1.3
$\chi_{\phi;\ ion-1,\ ion-2,\ el}^{gyro}$ $[(c_s/a)\rho_s^2]$	0.4, 0.1, 0.0	0.5,-0.1, 0.0	1.5,-0.0, 0.0	2.7,-0.0, 0.0
$D_{ion-1,\ ion-2,\ el}^{gyro}$ $[(c_s/a)\rho_s^2]$	0.7, 3.9, 0.3	0.3, 3.3, 0.1	0.2,-1.2, 0.2	0.8, 1.4, 0.7
Γ_E^{gyro} [MW]	8	4.2	16	8.5
Γ_ϕ^{gyro} [Nt-m]	6	-4.0	32	39
Γ_{el}^{gyro} [MW/keV]	-0.03	-0.01	0.02	0.0

Table 1: *ELMy H-mode plasmas, times and radii studied, transport from TRANSP power-balance and from GYRO turbulence simulations*

Methods - The TRANSP analysis code was used to compute the energy, particle, and momentum flows from measured plasma profiles using local conservation and calculated source profiles. Several transport parameters from TRANSP analysis are given in Table I for comparison with the GYRO simulation results. The energy transport is dominated by conduction in the plasma domains we consider. Other energy loss mechanisms, such as radiation and charge exchange, are excluded. We computed E_r for input to GYRO from force balance using the measured $\nabla(p_{carbon})$, v_{tor}, and the relatively small values for v_{pol} calculated using the NCLASS code [6] in TRANSP. E_r and, $\nabla(E_r)$ (a proxy for the shearing rate $\gamma_{E\times B}$ are given in the Table.

The GYRO code was used with extended radial domain, kinetic electrons and multiple ion species to simulate ITG and TEM modes. For the runs reported here, inputs with two ion species were used. The main ion species is the bulk ion, deuterium for three of the plasmas, and an average of the thermal DT for JET 42982. The second species

is the impurity and beam ion densities combined to maintain local charge neutrality. For three of the plasmas, the impurity density is the measured carbon density. For JET 53030, it is the measured Carbon and Argon densities combined.

The runs were performed using 384 CPU's on an IBM SP RS/6000 (Seaborg) and 128 on a dual AMD Opteron 248 cluster (Jacquard), both at NERSC, and 64 on an IBM p690 system (Cheetah) at ORNL. The number of toroidal modes was 16. Typically the range of $k_\theta \rho_s$ was 0-0.9 ($n_{toroidal}$ up to about 200) to cover the ITG and TEM region. Typically 100-200 radial and poloidal grid points were included, and the box sizes were about 100 ρ_s x 100 ρ_s.

Linear runs were done to find the linear growth rates γ_{lin} and mode frequencies ω_{lin} versus $k_\theta \rho_s$. The maximum γ_{lin} and corresponding ω_{lin} and $k_\theta \rho_s$ are given in the Table. All cases have negative ω_{lin}^{gyro} indicating rotation in the ion-drift direction. The values for the $E \times B$ flow shearing rates are also given, for comparison with γ_{lin}^{gyro}. Most of the nonlinear runs were done in the electrostatic approximation. One set of runs was done with the full electromagnetic terms and reduced, but non-zero β_e. These corrections to the simulated electrostatic levels of transport were negligible.

Nonlinear GYRO Results - The nonlinear runs start in a linear regime with negligible turbulence, and evolve into a regime where the zonal flows ($n_{toroidal} = 0$) and $n_{toroidal} > 0$ flows compete. Transitions from different quasi-steady-state regimes can occur, so the runs need to be continued for long times ($t \gg 500[a/c_s]$) to establish steady-state levels of transport. Examples of GYRO results are given in Table I and shown in Figs. 1-2. The χ values are given in units of $(c_s/a)\rho_s^2$. The energy fluxes for all the cases are dominated by ions with $\Gamma_E^{ion}/\Gamma_E^{el} \simeq 10$.

Since the plasmas are close to marginal stability, the transport depends sensitively on plasma parameters such as $\nabla(T_i)$ and $\nabla(E_r)$. Ten percent reductions in $|\nabla(T_i)|$ can typically drop energy flows by at least 2-fold. Thus it is of special interest to compare the relative magnitudes of the simulated transport coefficients. For the DIII-D plasmas the simulated energy $(\Gamma_E^{ion} + \Gamma_E^{el})$ and momentum flows with nominal $\nabla(T_i)$ and $\nabla(E_r)$ are higher than the TRANSP values by factors greater than 2. We used variations of $|\nabla(T_i)|$ and $|\nabla(E_r)|$ to achieve approximate agreement for the energy flow, and found that the momentum flow also agreed, i.e., $\Gamma_\phi^{gyro}/\Gamma_E^{gyro} \simeq \Gamma_\phi^{transp}/\Gamma_E^{transp}$.

The GYRO runs for the JET plasmas with nominal values for $\nabla(T_i)$ and $\nabla(E_r)$ predict low transport. Reducing $|\nabla(E_r)|$ 10 % was sufficient to get approximate agreement with the measured energy flow for the DT plasma, but the simulated momentum flow was high by a factor of 2. For the JET Ar injection shot reducing $|\nabla(E_r)|$ by a factor of four resulted in approximate agreement for the energy flow, but the momentum flow remained to high by a factor of 4.

The simulated energy transport coefficients for the bulk ions, impurity+beam ions, and electrons are given in the Table by $\chi_{E;\ ion-1,\ ion-2,\ el}^{gyro}$. The simulated species transport is given analogously by $\chi_{\phi;\ ..}^{gyro}$, (with negligible momentum carried by the electrons). The simulated species transport is given analogously by $D_{...}^{gyro}$.

The spectra of the energy and species flows versus $k_\theta\ \rho_s$ have peaks around 0.3, shown in Figs.1. The electron particle flow is simulated to be close to zero, as given by TRANSP. Note that Fig. 1-b indicates that the particle flows have complicated dependencies on $k_\theta\ \rho_s$. This implies that gyrokinetic analysis is needed to fully understand particle flows. The profiles of the energy and angular momentum flows are shown in Fig. 2. For the run shown $|\nabla(E_r)|$ was reduced 10% below its nominal value. This increased the simulated energy flow by a factor of two, resulting in approximate agreement with TRANSP, as shown in Table I. The energy flow is close to the TRANSP-measured value in Table I, but the angular momentum is too high by a factor of 2.5.

Discussion and Summary - The GYRO simulations with the nominal $\nabla(T_i)$ and $\nabla(E_r)$ over-predict the energy and momentum transport in the DIII-D plasmas and under-predict in the JET plasmas at the times and radii studied. It is possible that more accurate simulations of the energy, angular momentum, and species flows could be achieved with GYRO using more than two ion species. The procedures for generating appropriate inputs from TRANSP archives have been developed, but the runs have not

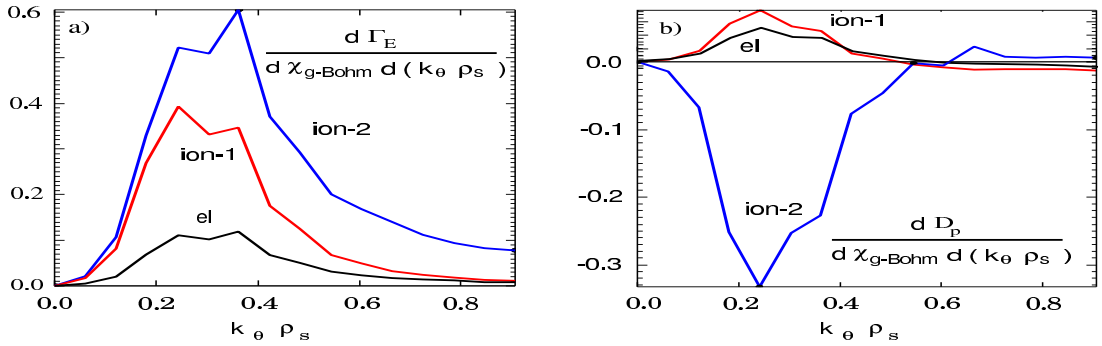

Figure 1: Spectra of a) energy and b) particle transport in JET 42982 from GYRO

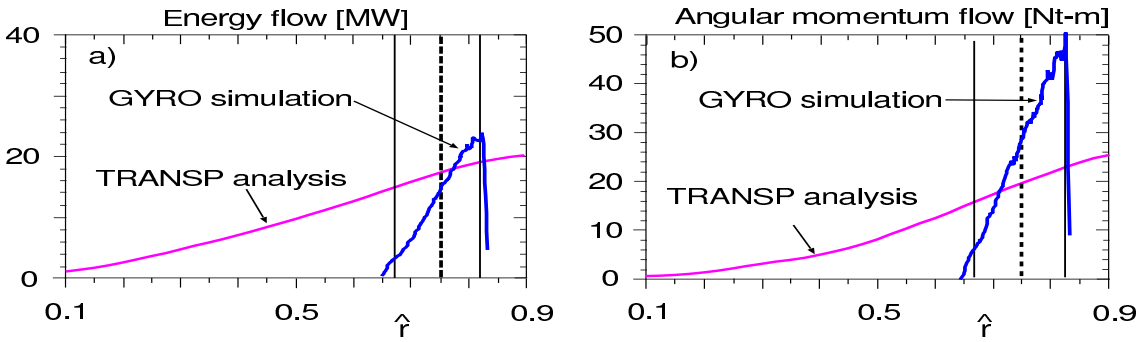

Figure 2: Profiles of a) total energy and b) angular momentum flow for JET 42982 from the TRANSP analysis and GYRO simulation

been started yet, due to dearth of CPU. Another possible explanation of the discrepancy is that the values of $\nabla(E_e)$ are incorrect. For instance, if v_{pol} differs considerably from the neoclassical predictions, then its contribution could be significant. An enhancement of $|\nabla(E_r)|$ would be needed for the DIII-D plasmas and a reduction for JET.

Actual transport in the core can be higher than a local prediction due to the nonlocal transport effects of turbulence spreading from the more unstable edge [7-9]. Based on a simple nonlinear model of turbulence spreading [9], this effect is more pronounced in devices and regions with higher ρ_s. It is not clear how this mechanism could reconcile the under-predictions in JET and over-predictions in DIII-D.

The GYRO-simulated ratios of the magnitudes of the angular momentum and energy flows are consistent with measurements for the DIII-D plasmas, but are high for the JET plasmas. The toroidal velocities for the angular momenta of both ion species were assumed to be equal to the values measured for the carbon impurity. Perhaps a more accurate procedure would result from using this velocity only for the impurity ions and using the toroidal velocity calculated from neoclassical theory for the angular momentum of the bulk ions.

We wish to thank R.Andre, D.Mikkelsen, and R.Groebner for assisting in this work which was conducted under the US DoE Contract No. DE-AC02-76CH03073.

*See the Appendix of J.Pamela *et al.*, Fusion Energy 2004 (Proc. 20th Int. Conf. Vilamoura, 2004)

[1] J.Candy and R.E.Waltz, Phys. Rev. Letters **91** (2003) 045001-1
[2] C.Estrada-Mila, J.Candy and R.E.Waltz, Phys. Plasmas **12** (2005) 022305
[3] C.C.Petty, M.R.Wade, J.E.Kinsey, D.R.Baker, and T.C.Luce, Phys. Plasmas **9** (2002) 128
[4] R.V.Budny, D.R.Ernst, T.S.Hahm, D.McCune, *et al.*, Phys. Plasmas **7** (2000) 5038
[5] J.Ongena, P.Monier-Garbet, W.Suttrop, Ph.Andrew, *et al.*, Nuclear Fusion **44** (2004) 124
[6] W.Houlberg, K. Shang, S. Hirshman, and M. Zarnstorff, Phys. Plasmas **4** (1997) 3230.
[7] R.E.Waltz, J.Candy, and M.N.Rosenbluth, Phys. Plasmas **9** (2002) 1938.
[8] R.E.Waltz and J.Candy, to appear in Phys. Plasmas **12** (2005)
[9] T.S.Hahm, P.H.Diamond, Z.Lin, *et al.*, to appear in Phys. Plasmas **12** (2005)